Investigation of defect states in heavily dislocated thin silicon films

T. Mchedlidze[1,a)] and M. Kittler[1,2]
[1]*Jointlab IHP/BTU, Konrad-Wachsmann-Allee 1, D-03046 Cottbus, Germany*
[2]*IHP microelectronics, Im Technologiepark 25, D-15236 Frankfurt (Oder), Germany*

(Received 13 December 2011; accepted 30 January 2012; published online 8 March 2012)

Deep level transient spectroscopy (DLTS) and photoluminescence (PL) were applied for investigation of defect states in thin crystalline silicon (Si) films deposited on glass. The films were fabricated by solid phase crystallization of amorphous Si layers and subsequently were subjected either to rapid thermal annealing or/and to hydrogenation. The study revealed presence of carrier traps and radiative recombination centers characteristic for dislocations in Si. Density of the traps strongly varied depending on the fabrication processes applied to the film. This allowed to link formation of the defects with applied fabrication processes and suggested origins for the traps. Passivation of the dislocation-related defect states by hydrogen was observed and appearance of hydrogen-related traps for the dislocated structures was detected. An increase in intensity of dislocation-related luminescence well correlated with the decrease in density of deep dislocation-related traps. © *2012 American Institute of Physics*. [http://dx.doi.org/10.1063/1.3692745]

I. INTRODUCTION

Investigation of defect states in silicon samples containing dislocations has long history (see, e.g., Kveder *et al.*[1] for the latest review). Continuous interest to dislocations in Si is based on several aspects. First, these defects are always present in Si lattice in certain density. The range of the densities comprises several orders of magnitude from less than 10^3 cm^{-2} for high quality monocrystalline material to more than 10^9 cm^{-2} for thin Si films fabricated in solid phase crystallization mode. Second, dislocations reveal electrical and radiative activity, thus strongly influencing relevant properties of Si. Dislocations also affect plastic properties of the material. Third, dislocations interact with other defects present in the lattice, thus affecting their properties. Last but not least, dislocations and their assemblies can be controllably introduced in Si and applied for engineering of Si material with advanced properties.[1,2]

Dislocations in Si present broad class of complicated objects with variations in structural and electrical properties.[1] Interaction of dislocations with native and impurity atoms, precipitates and structural defects cause further complications in their properties. Forming dislocations with similar properties in the samples can present useful approach for study of such complex structures. Namely, dislocation networks (DN) formed by direct bonding of Si wafers[2] were recently applied for study of dislocation-related defect states. Since the direct bonding forms networks containing particular type of dislocations[3] it was possible to attribute certain optical[4] and electrical[5] properties to particular dislocation structures. On the other hand DNs can be explicitly characterized by transmission electron microscopy (TEM).[3] Data obtained for DN can be applied for description of properties of grain boundaries (GB) in multicrystalline Si. However, from the experiments with DNs it also became clear that density of dislocations and their interaction play definitive role in the properties of the material.[4,5] Therefore properties of heavily dislocated Si material deserve separate investigation. Moreover, thin Si films on glass formed by various crystallization methods and containing dislocations in high density are broadly applied recently in large scale electronics and photovoltaics (for a review, see e.g., Shah *et al.*[6]).

One of the first publications about heavily dislocated Si reported on measurements of DC conductivity, Hall effect and photoluminescence (PL) along with TEM investigations.[7] Dislocations in high density were introduced in Si by plastic deformation (with shear strain up to 35%) performed at very high temperatures (~1300 K). Dislocation density in the deformed samples reached 1–5 × 10^9 cm^{-2} values. PL signal detected at 4.2 K contained D1–D4 peaks attributed previously to dislocation states in Si.[8] The results of Hall effect measurements suggested existence of defect states separated on 0.3–0.4 eV from valence and conduction bands. Structures formed during solid-phase crystallization (SPC) of Si present another type of heavily dislocated material. Recently such material was used in Crystal Silicon on Glass (CSG) thin film (TF) technology for PV-cell production.[9,10]

The CSG technology for TF solar cell production comprises successive deposition of SiN (several tens of nm thick) and amorphous Si (*a*-Si, 1.4–1.8 μm thick) layers on a textured glass substrate. The thin SiN layer serves as a barrier for impurity diffusion between glass and Si during processing and as an antireflection coating in future solar cells. The *a*-Si layer is transformed into polycrystalline-Si during SPC process. The SPC process is followed by rapid thermal annealing (RTA), which reduces density of structural defects in the material and activates dopant atoms. Subsequent annealing in hydrogen atmosphere reduces the electrical activity of remaining defects. Finally, the TF material is structured and electrical contacts are fabricated for the solar

[a)]Author to whom correspondence should be addressed. Electronic mail: teimuraz.mtchedlidze@physik.tu-dresden.de. Present address: Technische Universität Dresden, D-01062 Dresden, Germany.

cells.[10] Density of dislocations in the material estimated from TEM investigations was at the level of $\sim 2 \times 10^9$ cm^{-2}.

Properties of the TF CSG material was recently investigated using photoluminescence (PL).[11–13] Along with strong PL signal of dislocation-related luminescence (DRL), weak band-to-band luminescence (BBL) was also detected.[11] The characteristics obtained using PL was compared to the performance of the PV cells fabricated using the similar material and showed a capability of DRL to evaluate the quality of the material at different fabrication stages.[12] Moreover, it was shown that variation in the fabrication processes could strongly influence DRL signal from the film and that DRL can be used as an in-line monitoring tool for the film quality.[13] First DLTS results obtained from the CSG thin films were also reported recently.[14]

In the present report we compare PL and DLTS results obtained for the CSG TF samples fabricated with variations in the standard fabrication processes. As a result it was possible to ascribe detected defect states to the particular processes of the film formation and clarify influence of hydrogenation.

II. SAMPLES AND EXPERIMENTAL DETAILS

CSG-solar AG provided the samples for this study. Details about the standard CSG film fabrication and structure can be found elsewhere.[9,10,12] A description of the structure of the electrical contacts was also presented previously.[15] The samples contained highly boron-doped p^+ layer serving as a back surface field, moderately boron-doped light-absorber layer p^- and highly phosphorous-doped n^+ layer (see Fig. 1). Aluminum (Al) contacts were deposited after formation of the film and contacted p^+ and n^+ volumes. The diode areas ($\sim$0.27 mm^2) used in DLTS measurements, were separated from the continuous CSG film by laser patterning [see Fig. 1(a)].

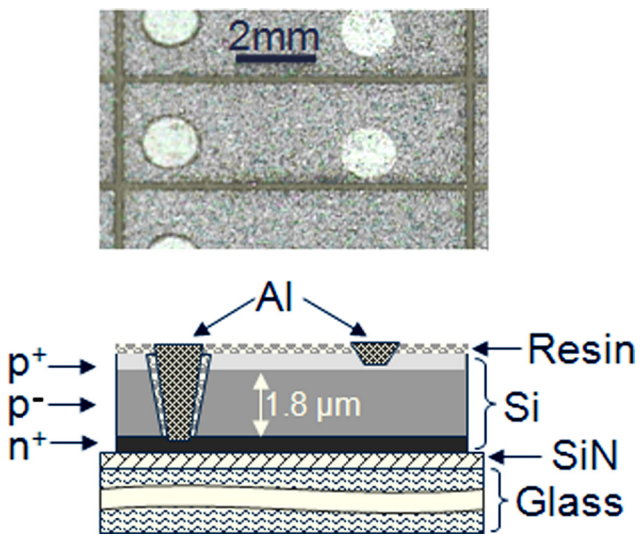

FIG. 1. (Color online) Magnified top image (up) and a sketch of the cross-section (down, not to the size) of a diode structure (CAH sample) used for DLTS measurements. The structures were separated from the continuous CSG film by laser patterning seen in the image as vertical and horizontal lines.

Four types of samples were fabricated for the investigation. The first type, labeled "CAH" contained Si film subjected to all standard processes used in the fabrication of CSG solar cell modules. Namely, after Si deposition the film was consequently crystallized in SPC mode (C), then it was subjected to fast, high-temperature annealing (A) and the residual defects were passivated by annealing in hydrogen (H).[9,12] For the second type of the samples the high-temperature annealing step (A) was skipped; these samples will be labeled "CH." The third type of the samples was not subjected to hydrogenation (H); these samples will be labeled "CA." The fourth type of samples labeled "CAHH" were additionally hydrogenated after laser patterning.

DLTS measurements were performed by means of a transient Fourier spectroscopy system DL-8000 (Accent) working at the capacitance testing frequency of 1 MHz. Principles of the method and the system were previously described.[16] A depletion region in the diode with low population of excited carrier traps is formed by applying reverse bias, U_R across the junction. The population of the traps is altered by application of a "filling" pulse, U_P with t_P duration. After finish of the filling pulse, a capacitance transient of the diode, initiated by thermal excitation of carriers from the traps to the nearest band is registered during sampling time t_W. The capacitance transients registered during temperature scan are digitalized and the discrete Fourier coefficients are calculated from the Fourier transformation of each transient data. A temperature dependence of amplitude of Fourier coefficient constitutes DLTS spectrum, where position of each peak maximum corresponds to a coincidence of emission time constant of a trap with the rate window, related to the corresponding Fourier coefficient. The DLTS spectrometer was equipped with closed circle helium cooling system, which allowed measurements of the samples in 30–320 K temperature range. Samples were protected from nonequilibrium illumination during the measurements.

PL was excited from the side of the Si film with a frequency doubled Nd:YVO_4 laser producing cw radiation at a wavelength of 532 nm. A spot diameter for PL excitation was $\sim$100 μm and radiation power was varied in the range 20–200 mW. PL signals were analyzed with a monochromator with the spectral resolution of 2 nm and registered by N_2 cooled Ge detector. Chopping of excitation light at a frequency of $\sim$30 Hz and subsequent lock-in detection were used to increase the signal-to-noise ratio. The registered PL spectra were corrected to the spectral response of the optical setup. The PL measurements were conducted at 80 and 300 K. For measurements at 80 K a sample was placed inside N_2-flow Oxford cryostat. Mapping of PL signal intensities across the sample area was performed at the DRL-signal maximum, i.e., at $E_{ph} = 0.795$ eV, by scanning of the excitation beam across the sample area with step $\Delta x = \Delta y = 0.2$ mm.

III. RESULTS

A. DLTS measurements

Results of static current-voltage (IV) and capacitance-voltage (CV) measurements for the samples were presented previously.[14] All samples revealed diode-like IV characteristics.

Leakage current in reverse direction was the largest for CAH sample and the smallest for the CH sample. Doping profiles for the absorber volume recalculated from the *CV* measurement data showed nearly constant value $\sim 2.6 \times 10^{15}$ cm^{-3} for CH sample. For the other samples dopant concentration varied from 8×10^{15} cm^{-3} to 6×10^{14} from top to bottom (according to the sketch in Fig. 1) of TF absorber. Obviously the variation of dopant concentration was related to indiffusion of dopant atoms during annealing step at 900 °C.

DLTS spectra detected from the samples are presented in Fig. 2. Note, that the measurement parameters were the same for all samples. For the spectra presented in Fig. 2(a) the sampling time was 100 ms, while it was 10 ms for the spectra in Fig. 2(b). As seen from the figures, the samples contain similar traps but in substantially different densities. Moreover, a peak with negative sign positioned at ~270 K could be seen in the spectra of CH sample. For DLTS measurements using *pn*-junctions, "negative" peaks may correspond to the minority carrier traps. Since filling of minority carrier traps should increase with the increase of the current through the diode during the filling pulse, their amplitude should strongly increase in the case of pulse (U_p) with the sign corresponding to direct current, while the depletion bias (U_R) remains the same. The measurements performed applying $U_p < 0$ V revealed that minority carrier traps were present in all samples. An example of the DLTS spectrum detected under various applied pulse conditions for the CA sample is presented in Fig. 3(a) as an example.

In total, seven majority carrier (hole) traps, i.e., Ta1–Ta7 were detected in the samples. Note that for the Ta4 the position of the peak maximum in the CH sample is influenced, i.e., is shifted to lower temperatures, by the neighbor negative peak. Such influence becomes obvious from the change in actual position of Ta4 peak maximum for the various U_p in Fig. 3(a), observed in this case for the CA sample. Correct identification of the extreme positions for the negative peaks is burdened by the presence of the peaks related to majority carrier traps. This becomes obvious if one compares CA and CA* spectra in Fig. 3(b). Note that for CA* spectrum the

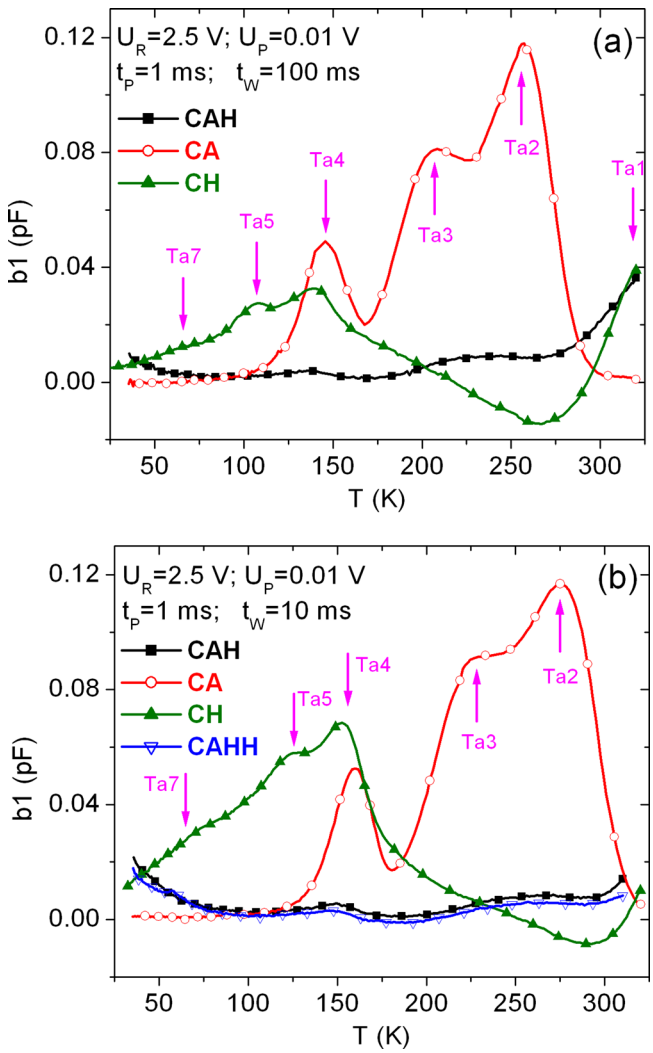

FIG. 2. (Color online) DLTS spectra detected from the samples for sampling times 100 ms (a) and 10 ms (b). Attribution of the curves and measurement conditions are indicated in the figures. Measurement parameters: U_R is reverse bias, U_p – bias during the filling pulse, t_W – sampling time and t_p – pulse duration. Vertical arrows show positions of the peaks for the detected traps Ta1–Ta7.

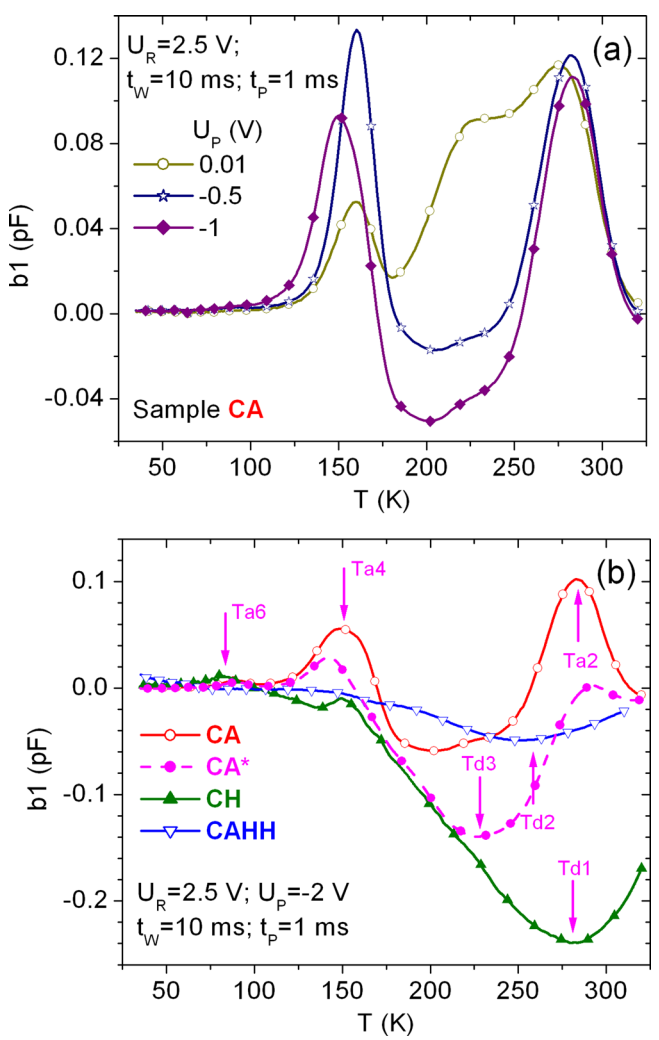

FIG. 3. (Color online) DLTS spectra detected in CA sample under various pulsing conditions (a) and those detected in various samples under the same negative pulse conditions (b). The spectrum labeled CA* corresponds to that of CA with subtracted spectrum for the same sample but with $U_p = 0.01$ V. Attribution of the curves and measurement conditions are indicated in the figure.

values detected at $U_p = 0.01$ V were subtracted from those for $U_p = -2$ V. However, for the investigated samples the extreme positions of these negative peaks were in the range of temperatures 225–275 K under the experimental conditions shown in Fig. 3(b). The parameters for the negative peaks coincided for the samples CAH and CAHH (Td2 trap). Trap parameters detected for CA (Td3 trap) and for CH (Td1 trap) differed from Td2 [see Fig. 3(b)].

For Ta2 – Ta7 traps it was possible to estimate position of the related levels in the bandgap ($E_t - E_V$) and of carrier capture cross-sections (σ) from the Arrhenius plots obtained from the results of the temperature scans for the samples. Similar procedure was applicable for the levels related to minority traps; however the precision of such estimations was lower due to superposition of the peaks from majority traps.

For Ta1 trap temperature scans gave scattered results due to the long sampling time, t_W, required for the detection of the peak. Therefore, it was decided to obtain parameters of this trap from the series of isothermal measurements with variation of t_W.[16] DLTS spectra were detected for scan of t_W from 2×10^{-4} to 20 s at static temperatures from 285 to 320 K with difference of 5 K between each measurement step. The obtained Arrhenius plots for all detected traps are presented in Fig. 4 and the parameters of the traps are summarized in Table I.

Estimations of correct values for the trap densities in the case under consideration are complicated. First, the obtained large gradient of dopant concentrations in the samples requires profiling of the trap densities. This task could not be completed in the present study since the actual Al contacts were unable to tolerate more than single temperature scan cycle. Probable reason for that could be in the influence of the low measurement temperatures on the isolation resin (see sketch in Fig. 1). The second reason is more general and is related to the extended character of the defects responsible for the traps in the samples under consideration. As it was shown previously,[17,18] for the extended defects, i.e. dislocations, grain boundaries, precipitates, etc., determination of the trap density from DLTS spectra requires knowledge of the character of the defect states (band-like and/or localized). Since the required information is unavailable, estimations of trap density could not be performed. Therefore, we were able to compare only relative amplitudes of the peaks in DLTS spectra of the samples, detected under the same measurement conditions. The DLTS peak amplitudes are graphically presented in Fig. 5. Note that due to the large difference in the detected amplitudes of the peaks we used logarithmic scale for the amplitude axis.

B. PL measurements

Previous PL investigations of CSG samples showed good homogeneity of the PL signal intensity across the sample surface.[12,13] Moreover, good correlation was found between the DRL signal intensity and carrier lifetime for the samples.[13]

To check the homogeneity of the PL spectra inside the present samples, mapping of the DRL signal amplitude was performed for 5 mm^2 areas inside each sample. The maps

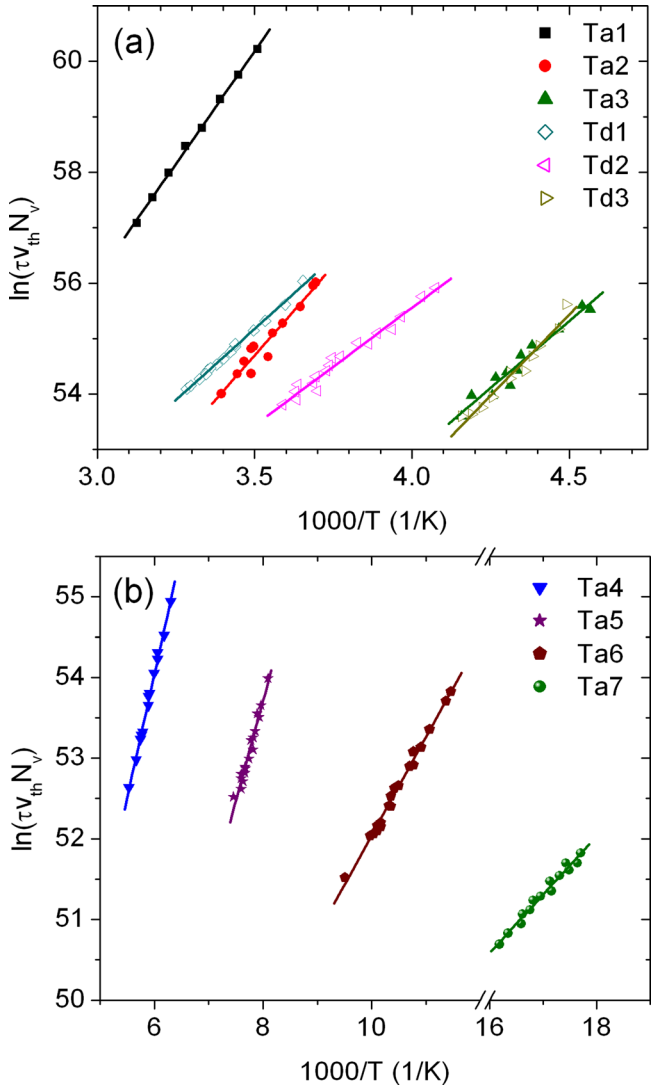

FIG. 4. (Color online) Experimental data (symbols) and fitted Arrhenius dependencies (lines) for deep (a) and shallow (b) traps detected in the samples.

TABLE I. Parameters of the traps obtained from the Arrhenius plots. In the rightmost column the samples are listed where the traps were detected. E_t (eV) represents the position of the trap level in the bandgap and σ (cm^2) represents carrier capture cross section. Note that for minority carriers (electrons) traps Td1–Td3 the results were strongly influenced by presence of majority carrier traps. This especially applies for the CA samples and the trap Td3.

Trap	E_t (eV)	σ (cm^2)	Sample
Ta1	$E_V + 0.7$	1.6×10^{-14}	CAH, CH, CAHH
Ta2	$E_V + 0.52$	5.1×10^{-15}	CAH, CA, CAHH
Ta3	$E_V + 0.41$	3.6×10^{-15}	CAH, CA, CAHH
Ta4	$E_V + 0.27$	6.8×10^{-16}	CAH, CA, CH, CAHH
Ta5	$E_V + 0.2$	1.0×10^{-15}	CH
Ta6	$E_V + 0.11$	1.0×10^{-17}	CAH, CA, CH, CAHH
Ta7	$E_V + 0.06$	2.6×10^{-17}	CAH, CH, CAHH
Td1	$E_C - 0.44$	1.4×10^{-16}	CH
Td2	$E_C - 0.37$	3.7×10^{-17}	CAH, CAHH
Td3	$E_C - 0.46$	5.2×10^{-14}	CA

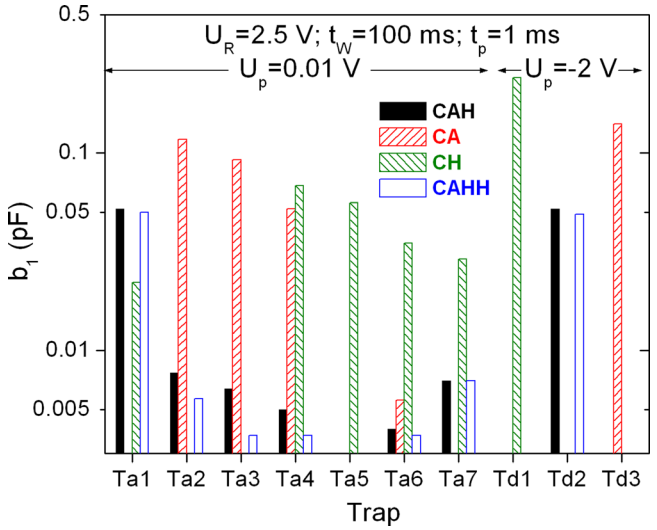

FIG. 5. (Color online) Amplitudes of DLTS peaks from the detected carrier traps. Measurements were performed with parameters indicated in the figure. Attribution of columns to the samples is indicated in the figure.

showed variations in within ~5% of the signal intensity. After that full PL spectra were detected for 10 arbitrary locations within each sample. The differences between the spectra were also insignificant. The final spectrum for each sample was obtained by averaging of the 10 local spectra. The resulting PL spectra, besides the film-related DRL and BBL peaks, contained peaks related to the substrate glass. Appearance of the substrate peaks in the spectra, not detected in previous experiments[12,13] can be attributed to larger wavelength of the excitation beam used in the present investigation and to the related larger penetration depth of the excitation beam. To obtain spectra from the films, the substrate spectra were detected from the locations with removed film at the measurement temperatures and subtracted from the overall spectra. The PL spectra originating from the films detected from CAH, CA, CH, and CAHH samples at 80 and 300 K are presented in Fig. 6.

For all samples BBL was under detection limits for the spectra detected at 80 K. At 300 K BBL peaks were detected for CAH and CAHH samples, however since the maximum of the main substrate-related peak was positioned close to the BBL peak, i.e., at ~1.16 eV, the precision of the BBL peak shape and intensity was much less reliable than those for DRL peaks.

IV. DISCUSSION

From the previous investigations of CSG thin films,[9–13] the main carrier traps in the samples should be related to dislocations and/or to grain boundaries. Results of DLTS investigations of dislocations in Si are widely known (see, e.g., Seibt *et al.*[18] and references therein). However, in the case under investigation the samples contain large densities of dislocations. DLTS spectra from heavily dislocated volumes containing dislocation networks in directly bonded Si wafers were reported recently.[5,19] Comparison of the trap parameters for dislocation networks with those obtained in the present work immediately suggests that traps Ta2, Ta3, Ta4, and

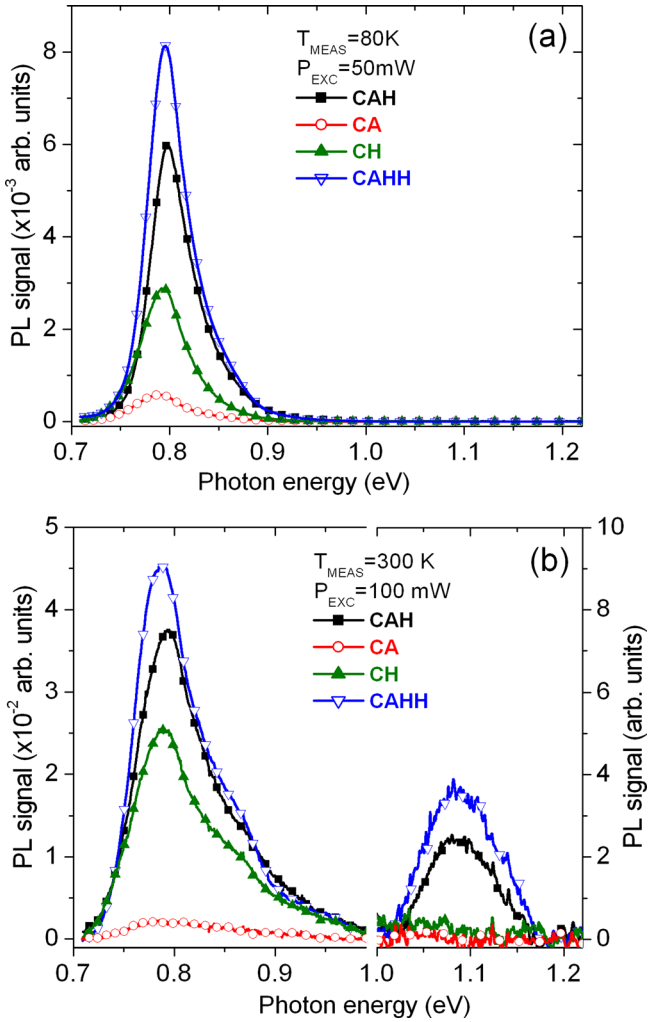

FIG. 6. (Color online) PL spectra detected from the samples at 80 K (a) and at 300 K (b). Attribution of the curves and experimental conditions are presented in the figures. Note different magnification coefficients for the signal amplitudes between (a) and (b) and between different parts of spectra in (b).

Ta6 could be attributed to dislocation structures. On the other hand, traps Ta1 and Ta7 are present only in the samples subjected to hydrogenation (see Fig. 5). Therefore it is valid to suppose that these traps are related to interaction of hydrogen with the structural defects in the TF material.

The samples subjected to hydrogenation procedure, i.e., CAH, CAHH, and CH, showed presence of the Ta1 trap. Contrary, this trap was not observed for CA sample and, to our knowledge, was not associated with dislocation structures previously. Moreover, since CH sample was not subjected to high-temperature annealing procedure, sufficient role of contamination atoms in formation of the Ta1 trap also can be excluded. Therefore, we suppose that the Ta1 trap presents result of interaction of hydrogen with some dislocation structures.

Densities of Ta2 and Ta3 traps are sufficiently lower in CAH and CAHH samples in comparison to CA sample. Therefore, we can suggest that electrical activity of these traps was substantially suppressed by hydrogenation. Such passivation of active dislocation-related traps well agrees with previously published investigations (see Seibt *et al.*[18] and references therein). Interestingly, in the CH sample these

traps were not observed. This may suggest some structural changes for dislocations that were induced by the 900 °C annealing step after crystallization, leading to formation of defect states responsible for Ta2/Ta3. On the other hand, influence of contamination during high-temperature annealing on the activation of already existing defect structures[18] cannot be excluded as well. The Ta5 trap was observed only in CH sample which was not subjected to the high-temperature annealing step. Therefore we can suppose that the annealing step destroys the centers responsible for the Ta5 trap. Influence of hydrogen on formation of this trap also could not be excluded.

Performed PL investigations suggested that the main radiative transition for the samples corresponds to D1 DRL peak with energy maximum at $E_{ph} \approx 0.8$ eV. From the previous publications,[20,21] carrier transitions causing D1 DRL peak should proceed through two, deep and shallow levels positioned in different halves of Si bandgap and separated from the nearest band by E_{dt} and E_{st} energies correspondingly. From the energy considerations we should expect that:

$$E_{dt} + E_{st} + E_{ph} \approx E_{BG}, \quad (1)$$

where $E_{BG} \approx 1.16$ eV presents bandgap energy for Si. From Eq. (1) and from the data in Table I we can expect that Ta4 and Ta6 traps were related to D1 DRL peak. Moreover, only Ta4 and Ta6 traps were detected in all of the measured samples (see Fig. 5) and all of the samples showed presence of D1 DRL peak. Note that both Ta4 and Ta6 are majority carrier traps, therefore the traps belonging to the lower half of the bandgap. To fulfill the above supposition and Eq. (1), the pair of the traps should belong to the different halves of the bandgap. We were not able to detect the "mirror," electron traps for Ta4 and/or Ta6 in our experiments. However presence of Td1–Td3 electron traps supports possibility of their existence. Presence of mirror traps in Si with dislocations was suggested earlier in many publications (see, e.g., Kveder *et al.*[1]). Transitions between mirror shallow traps located near valence and conduction bands were accepted as origin for D3 and D4 DRL peaks.[20] Moreover, the defect states positioned symmetrically to the band edges were reported for heavily plastically deformed Si samples as well.[7] Recently existence of mirror traps in the samples with DNs was also reported.[22] All these facts support our supposition about involvement of Ta4 and/or Ta6 traps in D1 peak from DRL.

Large difference was observed between the intensities of DRL peaks detected from the samples (see Fig. 6). It will be interesting to correlate PL and DLTS results. A correlation of Ta4 and/or Ta6 trap signal amplitudes with DRL intensity was not obtained. As seen from Fig. 7, DLTS peaks of Ta4/Ta6 traps were much stronger for CA and CH samples where DRL signal was small and contrary, despite large DRL signal in CAH and CAHH samples, the detected Ta4/Ta6 DLTS signals were small. From the other hand, comparing Fig. 2 with Fig. 6 one notices that for CA, CAH, and CAHH samples intensity of DRL anti correlated with amplitudes of Ta2/Ta3 DLTS peaks. Therefore we can suppose that Ta2/Ta3 traps present the main nonradiative recombination (NRR) centers for the samples and suppress DRL. Absence of Ta2/Ta3 traps in CH sample than requires supposition about different NRR centers there. The Ta5 trap can be suggested for the role of the NRR center in the case of CH sample. Interestingly, sum of amplitudes for Ta2 and Ta3 traps for CA, CAH, CAHH samples and amplitude of Ta5 trap in CH sample well fits the anti correlation trend with the DRL signal intensity for the samples (see Fig. 7). It should be stressed that the above speculation was presented only as an example of possible explanation for the trend of DRL intensity for the samples. Moreover, undoubtedly minority carrier traps, only partly detected in our experiments, should play significant role in NRR processes and should be included in consideration for complete understanding of the recombination paths. However, we would like to stress interesting and important aspect suggesting that DRL intensity is strongly determined by NRR processes and even high density of DRL-related centers does not necessarily lead to stronger DRL intensity from the sample.

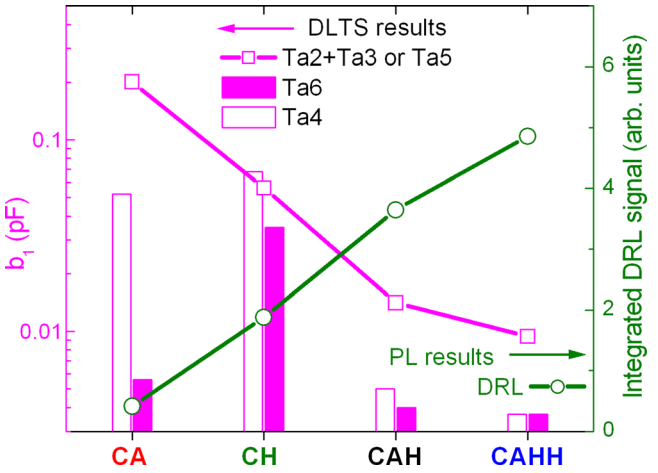

FIG. 7. (Color online) DLTS and DRL signal intensities for the samples. The attribution of symbols and columns are presented in the figure.

It is difficult to speculate about minority carrier traps observed in our samples, since their parameters and amplitudes of the peaks could not be determined with sufficient precision. However, it seems obvious that hydrogenation still sufficiently suppresses activity of these deep levels (see Fig. 7). Probably additional experiments will be necessary to clarify many aspects related to hydrogenation and to the electron traps in the samples.

V. SUMMARY

DLTS and PL analyses of thin crystalline Si films fabricated by solid-phase crystallization and subjected to various further treatments allowed to suggest origin for the defect states formed. Namely, it was possible to separate the carrier traps on groups related to crystallization, to high-temperature annealing and to hydrogenation. Moreover, it was possible relating some traps to NRR processes and suggesting DRL-active traps. Formation of deep NRR active traps during high-temperature annealing of the crystallized film and strong suppression of their activity by subsequent hydrogenation were observed. On the other hand, high-temperature annealing destroyed some of the traps existing

in the film after the crystallization process. It was also clearly shown that hydrogenation, while suppressing some of NRR centers, forms additional traps in the structure.

The results present a broad field for suppositions about dislocation structure in the CSG films, about possible transformation of the structure during RTA process, about impurity gettering by dislocations and about defect passivation. However, for the comprehensive analyses further investigations will be necessary. Since various crystallization processes of thin Si films on glass substrate, such as laser crystallization, electron-beam induced crystallization, layer exchange, etc., forms structures with high dislocation densities, the obtained results present substantial interest.

ACKNOWLEDGMENTS

We would like to thank J.-H. Zollondz and J. Schneider (CSG solar AG, Germany) for supply of the samples, for help with sample preparation and for useful discussions.

[1]V. V. Kveder and M. Kittler, Mater. Sci. Forum **590**, 29 (2008).
[2]M. Kittler, X. Yu, T. Mchedlidze, T. Arguirov, O. F. Vyvenko, W. Seifert, M. Reiche, T. Wilhelm, M. Seibt, O. Voß, A. Wolff, and W. Fritzsche, Small **3**, 964 (2007).
[3]M. Reiche, Mater. Sci. Forum **590**, 57 (2008).
[4]T. Mchedlidze, O. Kononchuk, T. Arguirov, M. Trushin, M. Reiche, and M. Kittler, Solid State Phenom. **156–158**, 567 (2010).
[5]M. Trushin, O. Vyvenko, T. Mchedlidze, O. Kononchuk, and M. Kittler, Solid State Phenom. **156–158**, 283 (2010).
[6]A. V. Shah, H. Schade, M. Vanecek, J. Meier, E. Vallat-Sauvain, N. Wyrsch, U. Kroll, C. Droz, and J. Bailat, Prog. Photovoltaics **12**, 113 (2004).
[7]S. A. Shevchenko, Yu. A. Ossopyan, T. R. Mchedlidze, E. A. Steinman, and R. A. Batto, Phys. Status Solidi A **146**, 745 (1994).
[8]N. A. Drozdov, A. A. Patrin, and V. D. Tkachev, JETP Lett. **23**, 597 (1976).
[9]M. A. Green, P. A. Basore, N. Chang, D. Clugston, R. Egan, R. Evans, D. Hogg, S. Jarnason, M. Keevers, P. Lasswell, J. O'sullivan, U. Schubert, A. Turner, S. R. Wenham, and T. Young, Sol. Energy **77**, 857 (2004).
[10]P. A. Basore, in Proceedings 21st European Photovoltaic Solar Energy Conference, Ed. J. Poortmans, H. Ossenbrink, E. Dunlop, and P. Helm (WIP, Munich, Germany, 2006), p. 544.
[11]T. Mchedlidze, T. Arguirov, M. Holla, and M. Kittler, J. Appl. Phys. **105**, 093107 (2009).
[12]T. Mchedlidze, T. Arguirov, S. Kouteva-Arguirova, and M. Kittler, Solid State Phenom. **156–158**, 419 (2010).
[13]T. Mchedlidze, J. Schneider, T. Arguirov, and M. Kittler, Phys. Status Solidi C **8**, 1334 (2011).
[14]T. Mchedlidze, J.-H. Zollondz, and M. Kittler, Solid State Phenom. **178–179**, 100 (2011).
[15]O. Breitenstein, R. Gupta, and J. Schneider, J. Appl. Phys. **102**, 024511 (2007).
[16]S. Weiss and R. Kassing, Solid-State Electron. **31**, 1733 (1988).
[17]M. Seibt, H. Hedemann, A. A. Istratov, F. Riedel, A. Sattler, and W. Schröter, Phys. Status Solidi A **171**, 301 (1999).
[18]M. Seibt, R. Khalil, V. Kveder, and W. Schröter, Appl. Phys. A **96**, 235 (2009).
[19]I. Isakov, A. Bondarenko, O. Vyvenko, V. Vdovin, E. Ubyivovk, and O. Kononchuk, J. Phys.: Conf. Ser. **281**, 012010 (2011).
[20]V. Kveder, M. Badylevich, W. Schröter, M. Seibt, E. Steinman, and A. Izotov, Phys. Status Solidi A **202**, 901 (2005).
[21]M. Kittler, T. Mchedlidze, T. Arguirov, W. Seifert, M. Reiche, and T. Wilhelm, Phys. Status Solidi C **3**, 707 (2009).
[22]A. Bondarenko, O. Vyvenko, I. Kolevatov, I. Isakov, and O. Kononchuk, Solid State Phenom. **178–179**, 233 (2011).